4946 J. Med. Chem. 2009, 52, 4946–4950
DOI: 10.1021/jm900434f

Journal of Medicinal Chemistry
Brief Article

X-ray Crystal Structure of Human Heme Oxygenase-1 with (2*R*,4*S*)-2-[2-(4-Chlorophenyl)ethyl]-2-[(1*H*-imidazol-1-yl)methyl]-4[((5-trifluoromethylpyridin-2-yl)thio)methyl]-1,3-dioxolane: A Novel, Inducible Binding Mode†

Mona N. Rahman,‡ Jason Z. Vlahakis,∥ Dragic Vukomanovic,§ Walter A. Szarek,∥ Kanji Nakatsu,§ and Zongchao Jia*,‡

‡*Departments of Biochemistry and* §*Pharmacology & Toxicology and* ∥*Chemistry, Queen's University, Kingston, ON K7L 3N6, Canada*

Received April 3, 2009

The crystal structure of human heme oxygenase-1 (HO-1) in complex with (2*R*,4*S*)-2-[2-(4-chlorophenyl)-ethyl]-2-[(1*H*-imidazol-1-yl)methyl]-4[((5-trifluoromethylpyridin-2-yl)thio)methyl]-1,3-dioxolane (**4**) reveals a novel, inducible binding mode. Inhibitor **4** coordinates the heme iron, with its chlorophenyl group bound in a distal hydrophobic pocket, as seen in previous structures. However, accommodation of the 5-trifluoromethylpyridin-2-yl group requires a significant shift in the proximal helix, inducing the formation of a hydrophobic pocket. This is the first example of an induced binding pocket observed in HO-1.

Introduction

The heme oxygenase (HO[a]) system comprises two active isozymes, namely, the inducible (HO-1) and the constitutive (HO-2); they catalyze the regioselective, oxidative cleavage of heme at the α-meso carbon to release ferrous iron (Fe^{2+}), carbon monoxide (CO), and biliverdin, the last being further transformed into bilirubin via bilirubin reductase (Supporting Information Figure S1).[1,2] This reaction is the main source of CO in mammals with ~85% of the CO produced in humans under normal physiological conditions being derived from heme. There has been increasing evidence of the cellular regulatory actions of CO including anti-inflammatory, antiapoptotic, antiproliferative, and vasodilatory effects.[3−6] Moreover, the HO system may have a protective role in several conditions including diabetes, inflammation, heart disease, hypertension, neurological disorders, organ transplantation, and endotoxemia.[7] HO-1 also has potential therapeutic applications in cancer, as its activity has been associated with the growth of most tumors.[8−10]

The use of selective HO inhibitors is crucial in the dissection of the CO/HO system and the mechanisms underlying its physiological effects and pathologies. They may also be beneficial in therapeutic applications. First-generation HO inhibitors have been metalloporphoryin-based and thus, because of their structural similarity to heme, have some degree of nonselectivity and toxicity. The discovery of azalanstat (**1**) (Figure 1),[2] which lacks the porphyrin nucleus of first-generation HO inhibitors, as a potent inhibitor of HO-1 and HO-2, led to a program in our laboratory aimed at the design of novel, isozyme-selective HO inhibitors. A structure−activity study was undertaken to systematically design and synthesize analogues of **1**, a process that resulted in a series of novel compounds, several of which have been shown to be potent HO-1 inhibitors.[11−15]

As part of our program, we have also undertaken a structural study of complexes formed between human HO-1 (hHO-1) and some of our selective HO-1 inhibitors using X-ray crystallography. We have reported the crystal structure of hHO-1 in complex with 1-(adamantan-1-yl)-2-(1*H*-imidazol-1-yl)ethanone (**2**)[16] which, in conjunction with the crystal structure of rat HO-1 in complex with another of our compounds, namely, (2-[2-(4-chlorophenyl)ethyl]-2-[(1*H*-imidazol-1-yl)methyl]-1,3-dioxolane (**3**),[17] revealed a common binding mode for these imidazole-based HO-1 inhibitors, despite having differing chemical features beyond the imidazolyl moiety (Figure 1). In general, the inherent flexibility of the hHO-1 distal helix allows the heme-binding pocket to expand to accommodate the inhibitor without displacement of the heme moiety, resulting in noncompetitive inhibition. Shifts in the proximal side of the pocket and with heme itself also contribute to this expansion to a lesser extent. The imidazole group serves as an anchor with the nitrogen at position 3 coordinating with the heme iron to result in a hexacoordinated heme. The western region of the inhibitor fits into a hydrophobic pocket on the distal side of the heme-binding pocket to stabilize binding further. The central region of the inhibitor, while close to the catalytically critical Asp140 residue, does not perturb its position. Rather, heme oxidation is inhibited via disruption of the ordered hydrogen-bonding network that Asp140 is involved in and, in particular, the ultimate displacement of the catalytically critical distal water ligand by the inhibitor.

Recently, we have published a study of imidazole−dioxolane compounds in which the effect of substituents at the 4-position of the dioxolane ring was analyzed, i.e., a series of analogues structurally more similar to **1**, as they included substituents in the northeastern region.[15] Most of these compounds were highly potent inhibitors of HO with moderate selectivity for HO-1. On the basis of the current structural knowledge, it was not clear how the northeastern substituents, which are rather bulky, would be accommodated by hHO-1. There are at least two possibilities: (i) hHO-1 undergoes a large conformational change to create a new binding subpocket; (ii)

*To whom correspondence should be addressed. Phone: (613) 533-6277. Fax: (613) 533-2497. E-mail: jia@queensu.ca.

†The hHO-1 complex structure has been deposited (PDB code 3HOK).

[a]Abbreviations: HO, heme oxygenase; Fe^{2+}, ferrous iron; CO, carbon monoxide; CHESS, Cornell High Energy Synchrotron Source; MR, molecular replacement; HP, hydrophobic pocket.

 Published on Web 07/14/2009

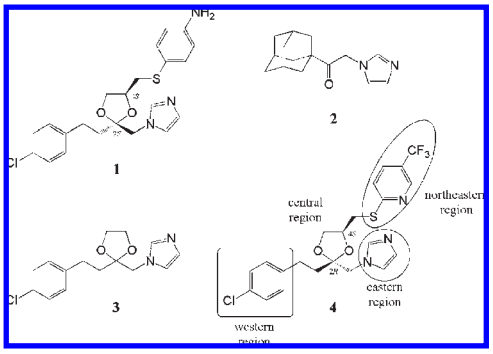

Figure 1. Structures of **1**−**4**.

this series of compounds assumes a different binding mode than that previously observed.[16,17] Either way, the binding would be novel. To reveal the binding mode, we carried out crystallographic studies and herein report the structure of hHO-1 with a representative example of these compounds, namely, (2*R*, 4*S*)-2-[2-(4-chlorophenyl)ethyl]-2-[(1*H*-imidazol-1-yl)methyl]-4[((5-trifluoromethylpyridin-2-yl)thio)methyl]-1,3-dioxolane (**4**) (Figure 1), which demonstrates for the first time the inhibitor-induced creation of a secondary, peripheral hydrophobic pocket, which can be formed to accommodate substituents in the northeastern region of our series of inhibitors.

Results and Discussion

Crystallization and Structure Determination of hHO-1 in Complex with 4. Initial screens using a CO formation assay with rat spleen microsomal fractions gave an IC_{50} of 2.1 ± 0.6 μM.[15] In comparison, the inhibitor that we previously cocrystallized with hHO-1, inhibitor **2**, had an IC_{50} of 7 ± 1 μM.[16] As such, the same methodology was undertaken to cocrystallize hHO-1 with **4**.[16]

To confirm binding of inhibitor **4** prior to setting up cocrystallization trials, spectral analyses were undertaken on the native protein and that incubated with inhibitor at a molar ratio of 1:3 for ~1 h. The Soret peak of the native protein incubated with inhibitor shifted to 413 nm, thus verifying binding (Supporting Information Figure S2). This mixture was subsequently utilized for crystallization trials based on and expanded from previous conditions.[16,18,19] The crystals formed were very similar to those obtained previously for native and hHO-1 in complex with **2**.[16] Diffraction data for the cocrystal were obtained to a resolution of 2.19 Å and assigned to the $P2_1$ space group. As the cell dimensions were different from those of previous crystal structures, molecular replacement was carried out using the native heme-conjugated hHO-1 complex (PDB code 1N3U) as the initial probe. Two unambiguous solutions were obtained corresponding to the two molecules in the asymmetric unit. The structure was refined to an R of 0.222 and an R_{free} of 0.289. A total of 186 water molecules was added to the structure. The Ramachandran plot demonstrated no residues in the disallowed region. The final statistics are given in Table 1.

It is noted that of the two molecules in the asymmetric unit, the B molecule had significant and unambiguous difference density that could be used to position the inhibitor. Moreover, we were able to detect an additional residue at the N-terminus (Met9), which had not been found in the native[18,19] or the inhibitor complexes[16] determined to date. In contrast, the density for the A molecule was somewhat weak. Following molecular replacement, clear difference density was observed

Table 1. Diffraction and Refinement Statistics[a]

space group	$P2_1$
a, b, c (Å)	55.07, 54.59, 71.88
β (deg)	94.64
molecules in the asymmetric unit	2
solvent content (%)	36.09
mosaicity (°)	1.95
resolution range (Å)	50−2.19
total reflections/unique reflections	64 747/19 662
completeness (%)	89.9 (68.8)
I/σ	17.3 (3.4)
R_{merge} [b]	0.098 (0.355)
average redundancy	3.3 (2.6)
Refinement Statistics	
σ cutoff for refinement	none
R_{crys} [c]/R_{free} [c]	0.222/0.289
no. of reflections: used/in test set	18614/1018
no. of non-hydrogen atoms used in refinement	3802
rmsd bond length (Å)/rmsd bond angle (deg)	0.007/1.047

[a] Values in parentheses are for the outermost shell (2.28−2.20 Å). [b] $R_{merge} = \sum|I_{obs} - \langle I\rangle|/\sum I_{obs}$, where I_{obs} is the intensity measurement and $\langle I\rangle$ is the mean intensity for multiply recorded reflections. [c] R_{cryst} and $R_{free} = \sum|F_{obs} - F_{calc}|/\sum|F_{obs}|$ for reflections in the working and test sets, respectively.

but it was disconnected, incomplete, and still somewhat weak. Further, there was not a similar shift in the proximal helix of the protein to accommodate the northeastern region of the inhibitor (data not shown). Thus, while there is partial density potentially corresponding to the inhibitor, we could not place this molecule with complete confidence. Moreover, a significant portion of the protein molecule was associated with weak density, making it difficult to resolve, which may indicate that there was still movement occurring in the A molecule as the protein tried to accommodate and bind the inhibitor. Indeed, analysis of the normalized *B*-factor values for each residue revealed that thermal factors in the region of the proximal helix were higher than the average for the molecule but also significantly higher than those of the equivalent region in the B molecule (data not shown). Comparison with the normalized values of the closed, i.e., putatively more active, conformation of the native structure (PDB code 1N45, chain A) revealed an increase in the thermal factor values in the proximal helix (data not shown); in contrast, there is a decrease in the relative values of the thermal factors in this region for the B molecule. Thus, it appears that the binding of the inhibitor may not have reached completion in the A molecule. As such, water was placed in the density corresponding to the partial density in this molecule. Given the ambiguity of this molecule, all further discussion will focus on the inhibitor-bound complex in the B molecule.

Overall Structure. In general, the overall structure of hHO-1 in complex with **4** (Figure 2A) is similar to that of the native heme-conjugated hHO-1 and to previous structures of hHO-1 in complex with analogous compounds.[16,17] The distal helix shifts outward in a similar manner to accommodate the inhibitor, although not to the same extent as to accommodate the bulky adamantyl group of **2** (Figure 3). In addition to these expected changes, there is a major conformational change involving the proximal helix to accommodate the bulky 5-trifluoromethylpyridin-2-yl group in the northeastern region of the inhibitor. Structures of the native holo and apo forms of hHO-1, as well as the holoenzyme in complex with **2**, reveal a sharp bend of ~60° in the proximal helix (Asn30 and Ala31) which is followed by a shorter helical segment from Glu32 to Lys39. From the complex structure with **4**, it appears that interaction with the

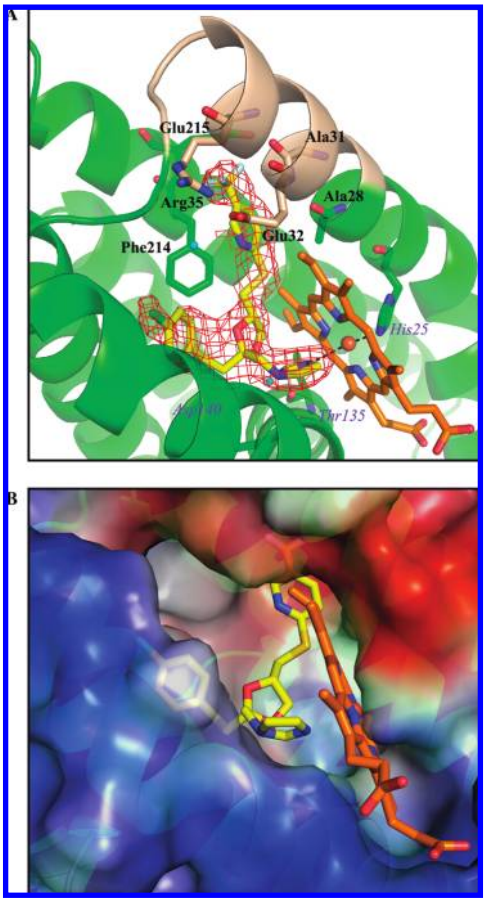

Figure 2. Crystal structure of hHO-1 in complex with **4**. (A) Ribbon diagram of the inhibitor-binding site at 2.19 Å resolution. Heme (orange) and **4** (yellow) are depicted as stick models. An omit map (red), contoured at 2σ, is shown. Dashed lines indicate coordination of imidazole nitrogens of **4** and His25 with the heme Fe. Residues within van der Waals distance of the northeastern region of **4** are indicated (black), as are the two water molecules involved in inhibitor stabilization, and select residues mentioned in the text (blue). Residues in the proximal helix that have been shifted because of inhibitor binding are highlighted (wheat). (B) Electrostatic surface potential of the inhibitor-binding site. Blue and red indicate positive and negative electrostatic potentials, respectively, as calculated using PyMOL.[29] The chlorophenyl moiety in the western region of **4** binds to the distal hydrophobic pocket in a manner similar to the binding of the analogous chlorophenyl moiety of **3**; the adamantyl moiety in the western region of **2** also binds to this distal hydrophobic pocket. The 5-trifluoromethylpyridin-2-yl group in the northeastern region of **4** fits into the secondary hydrophobic pocket. As such, the inhibitor-binding pocket in this complex is larger and more open than that seen for previous structures of HO-1 in complex with imidazole-based inhibitors.[16,17]

5-trifluoromethylpyridin-2-yl group causes residues in the region to be pushed back resulting in an "unkinking" and extension of the proximal helix up to Gln38. The northeastern group now occupies the hydrophobic space originally occupied by the thiol group of Met34 which has been shifted to the exterior of the newly formed pocket along with the functional groups of Phe33, Met34, Phe37, and Gln38. As well, the functional groups of Arg35 and Glu32 are shifted to the interior of the pocket and may be stabilized by an electrostatic interaction between the two side chains (2.25 Å). The magnitude of this change is exemplified by Gln38, which is shifted 10.76 and 11.79 Å relative to the native structure and the complex with **2**, respectively, while

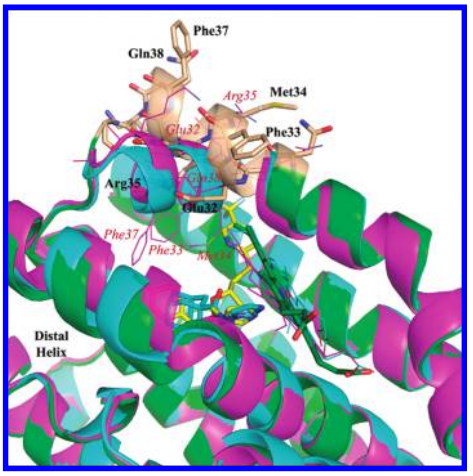

Figure 3. Structural alignment of hHO-1 in complex with **4** (green) with the native holoenzyme (PDB code 1N45, chain A, magenta) and of hHO-1 in complex with **2** (PDB code 3CZY, chain A cyan). Residues in the shifted proximal helix are highlighted as wheat stick diagrams (black labels), with corresponding residues in the native structure depicted as lines (italicized maroon labels). **4** is depicted in yellow.

Phe33 is shifted 8.01 and 9.03 Å, respectively (Supporting Information Figure S3). As seen by the electrostatic surface representation of the molecule (Figure 2B), binding of **4** results in further expansion, relative to the complex with **2**, to give a more open inhibitor-binding pocket.[16] The bulky northeastern region of the inhibitor is encompassed by another, newly formed, peripheral hydrophobic pocket. Residues lining this secondary hydrophobic pocket that make contributions to hydrophobic interactions include Ala28, Ala31, Arg35, Phe214, and Glu215 (Figure 2A). A detailed table of residues within van der Waals distance of the inhibitor, which contribute to its binding, is given in Supporting Information Table S1. Knowledge of the presence of charged groups within this region, such as Glu32, Glu215, and Arg35, may be utilized in the design of future compounds to further enhance the binding in this region.

In general, residues that contribute to the binding of other regions of the inhibitor are similar to those that have been demonstrated previously.[16] While most of the interactions contributing to inhibitor binding are due to hydrophobic interactions and metal coordination, hydrogen bonding may also contribute to the stability. One of the oxygens of the dioxolane group is close enough to a water molecule (3.48 Å) to form a potential, weak hydrogen bond. This water molecule may also be involved in a hydrogen-bonding network with the carbonyl group of Thr135 (2.61 Å), similar to what was observed in the crystal structure of rat HO-1 in complex with **3**.[17] In the secondary hydrophobic pocket, another water molecule is also in a potential hydrogen-bonding network involving the nitrogen of the pyridine ring in the northeastern region (3.49 Å) and with the carboxylate side chain of Glu32 (3.33 Å) to further stabilize the northeastern region of the inhibitor. As observed in previous complex structures, the binding of the inhibitor does not perturb the position of the catalytically critical Asp140 residue. Rather, HO-1 inhibition results from the disruption of the ordered hydrogen-bonding network involving Asp140 and from displacement of the critical distal water ligand required for heme oxidation.[18,19]

Induced Formation of the Proximal Hydrophobic Pocket. The significant conformational change observed in the proximal helix implies that there is a degree of flexibility associated

with this region that allows it to accommodate a bulky group in the northeastern region of a potential ligand. This was not apparent in previous structures of inhibitor−HO complexes which tended to focus more on the flexibility of the distal helix to open up the heme-binding pocket.[16,17] A potential, secondary hydrophobic pocket was noticed when analyzing our previous crystal structure of hHO-1 in complex with **2**.[16] This potential pocket is not apparent in structures of the native human[18,19] or rat HO-1 in complex with **3**.[17] Indeed, we were able to automatically dock **1**[16] and (2*R*,4*S*)-2-[2-(4-chlorophenyl)ethyl]-2-[(1*H*-imidazol-1-yl)methyl]-4-[(phenylsulfanyl)-methyl]-1,3-dioxolane[15] using the structure of hHO-1 in complex with **2** as a template such that the northeastern regions of the respective compounds fit into this potential pocket. However, our current complex structure demonstrates that there is a significant amount of conformational change involved in forming the secondary hydrophobic pocket, an aspect that could not have been anticipated from our previous work.

This unanticipated and significant conformational movement of the proximal helix led us to investigate this region more closely. Previous studies in which crystal structures of the apo and holo forms of hHO-1 were compared had indicated regions of large deviation in the proximal helix by plotting the rmsd for Cα atoms between the two holo and four apo forms.[19] Interestingly, the deviation reported between the holo and apo HO-1 forms was 1.8 Å, a value much lower than that observed upon binding of **4**. Moreover, a hydrogen-bonding interaction between the Nε atom of Gln38 and the carbonyl oxygen of the Glu29 backbone observed in the holoenzyme structure is absent in the apo form, which allows Gln38 to be quite flexible, its side chain adopting different conformations. The complex structure of hHO-1 with **4** reveals that the hydrogen-bonding interaction between Gln38 and Glu29 is also absent because of the shift of Gln38 away from the heme-binding pocket. A new hydrogen bond is formed between its backbone amide group of Gln38 and the carbonyl oxygen of Met34 (2.99 Å).

An analysis of the normalized temperature factors was performed to determine whether this region had an inherent flexibility similar to that seen with the distal helix and whether the distortion upon binding of the inhibitor caused it to become more flexible. A plot of the normalized *B*-factor values revealed that residues near the end of the proximal helix were slightly higher than the average for the molecule (0.5−1 standard deviations) (Supporting Information Figure S4A). However, a difference plot in which the normalized *B*-factors of the closed, i.e., putatively more active, conformation of the native structure (PDB code 1N45, chain A) were subtracted revealed a decrease in the thermal factors relative to the native structure, implying a decrease in flexibility (Supporting Information Figure S4B). It is noted that this proximal helical region of the native holoenzyme showed greater than average thermal factors (∼1−2 standard deviations) (Supporting Information Figure S4A), albeit not as high as those of the distal helix, which may imply some degree of flexibility in this region that is ultimately stabilized by interactions with the bulky 5-trifluoromethylpyridin-2-yl group of the northeastern region of **4**.

Conclusions

The binding of **4** to hHO-1 is very similar to that of other imidazole-based inhibitors that have been characterized to date.[16,17] However, accommodation of the bulky 5-trifluoromethylpyridin-2-yl group in the northeastern region requires a significant amount of conformational change to cause the formation of a secondary, peripheral hydrophobic pocket by "unkinking" and extending the proximal helix. As a result, this northeastern group occupies a hydrophobic space originally taken up by the thiol group of Met34, which is shifted to the exterior of the pocket. This newly formed hydrophobic pocket further stabilizes inhibitor binding mainly through hydrophobic interactions, although there appears to be a water molecule that may form a hydrogen-bonding network with the nitrogen of the pyridine ring and with the carboxylate side chain of Glu32. The conformational change also resulted in the rearrangement of several functional groups between the interior and exterior of this newly formed hydrophobic pocket. As such, the presence of Arg35 and Glu32 within the pocket may be exploited in future designs to strengthen binding in this region. The extent of formation of this secondary hydrophobic pocket could not be anticipated from previous structures of hHO-1 in complex with imidazole-based inhibitors that lacked this northeastern region.[16,17] Thus, this observation is an example of binding by "induced fit" in which the subpocket is formed by interaction with (in order to accommodate) the 5-trifluoromethylpyridin-2-yl substituent in the northeastern region of the inhibitor.

Experimental Methods

Synthesis. We have reported the synthesis of **4** hydrochloride in a previous publication.[15] The compound was determined to be >98% pure by elemental analysis (for C, H, and N) performed at MHW Laboratories (Phoenix, AZ) and was also characterized using ^{1}H and ^{13}C NMR spectroscopy and high-resolution electrospray mass spectrometry.

Expression and Purification of hHO-1. For crystallization purposes, a truncated, soluble version of hHO-1 was used that contains 233 amino acids (hHO1-t233) and has been employed successfully to solve the high-resolution crystal structure for hHO-1.[16,18−20] Bacterial expression and purification of hHO-1 were performed as described previously,[16] based on published protocols.[21−23]

Crystallization of hHO-1 in Complex with 4. Crystallization was performed using sitting-drop vapor diffusion as described previously,[16] based on published protocols.[18−20] The crystallization conditions consisted of 2.16 M ammonium sulfate and 1.15% 1,6-hexanediol in 100 mM HEPES (pH 7.25). The heme−hHO-1 complex (412 μM in 20 mM potassium phosphate) was mixed with **4** at a molar ratio of 1:3 and incubated for ∼1 h at room temperature. Binding was confirmed using spectral analysis to confirm a shift in the native Soret peak (from 403 to 413 nm) prior to setting up crystallization plates, as described previously.[16] Crystallization drops consisted of 2 μL of the protein−inhibitor solution mixed with 2 μL of the reservoir solution.

Data Collection and Structure Determination. X-ray diffraction data were collected at the A1 beamline of the Cornell High Energy Synchrotron Source (CHESS). For data collection a cryoprotectant comprising 100 mM HEPES (pH 7.25), 2.32 M ammonium sulfate, 1.15% 1,6-hexanediol, and 20% (v/v) glycerol was used. Crystals were subsequently flash-cooled in a stream of N_2 at 100 K. Data were collected for 180°, with an oscillation of 1°, and processed using HKL2000.[24] The structure of the protein−inhibitor complex was solved by molecular replacement (MR) using Phaser in the CCP4 suite;[25] the heme−hHO-1 complex (PDB code 1N3U) was the initial probe. An initial template of **4** was generated using CS Chem3D Ultra (version 6.0, Copyright 2000, CambridgeSoft.com) and the Dundee PRODRG2 server.[26] Following initial refinement with Refmac5, the structure of **4** was manually inserted in the B chain

and subsequently refined using iterative cycles of Xfit and Refmac5 in the CCP4 suite.[25] The refined B molecule was then superimposed onto the A molecule and the resultant structure further refined as previously described. Some rebuilding and refinement were also performed using PHENIX[27] and Coot.[28] Standard parameters for heme were used as described in its library entry in the program during refinement, with no additional restraints on planarity, bond lengths, and angles. Structural alignments and determination of contact residues were performed using CCP4.[25] Electrostatic surface potentials were calculated, and all images were prepared using PyMOL.[29]

***B*-Factor Analysis.** An analysis of the temperature factors was carried out as follows.[30,31] *B*-Factor values for the Cα atoms were normalized by the following equation:

$$B_i' = \frac{(B_i - B_{ave})}{\sigma}$$

where B_i is the *B*-factor for the Cα atom of residue *i*, B_i' is the normalized value, B_{ave} is the average of the B_i values over the whole molecule, and σ is the standard deviation.

Acknowledgment. This research was supported by CIHR. Z.J. holds a Canada Research Chair in Structural Biology. The X-ray data were collected at the Cornell High Energy Synchrotron Source. We thank Dr. Paul Ortiz de Montellano and Dr. John Evans (both from the University of San Francisco) for the generous gift of the hHO1-t233 plasmid and advice regarding its expression. We are grateful to Dr. Qilu Ye and Dr. Jimin Zheng for technical advice in structure determination.

Supporting Information Available: Results of oxidative degradation of heme in the carbon monoxide/heme oxygenase (CO/HO) pathway, spectral analysis of **4** binding to hHO-1, structural alignment, thermal factor analysis, and contacts between heme-conjugated hHO-1 and **4**. This material is available free of charge via the Internet at http://pubs.acs.org.

References

(1) Maines, M. D. The heme oxygenase system: a regulator of second messenger gases. *Annu. Rev. Pharmacol. Toxicol.* **1997**, *37*, 517–554.
(2) Vreman, H. J.; Wong, R. J.; Stevenson, D. K. Carbon Monoxide and Cardiovascular Function; CRC Press: Boca Raton, FL, 2002; p 273.
(3) Ryter, S. W.; Alam, J.; Choi, A. M. Heme oxygenase-1/carbon monoxide: from basic science to therapeutic applications. *Physiol. Rev.* **2006**, *86*, 583–650.
(4) Lee, T. S.; Chau, L. Y. Heme oxygenase-1 mediates the anti-inflammatory effect of interleukin-10 in mice. *Nat. Med.* **2002**, *8*, 240–246.
(5) Lee, T. S.; Tsai, H. L.; Chau, L. Y. Induction of heme oxygenase-1 expression in murine macrophages is essential for the anti-inflammatory effect of low dose 15-deoxy-delta 12,14-prostaglandin J2. *J. Biol. Chem.* **2003**, *278*, 19325–19330.
(6) Imuta, N.; Hori, O.; Kitao, Y.; Tabata, Y.; Yoshimoto, T.; Matsuyama, T.; Ogawa, S. Hypoxia-mediated induction of heme oxygenase type I and carbon monoxide release from astrocytes protects nearby cerebral neurons from hypoxia-mediated apoptosis. *Antioxid. Redox Signaling* **2007**, *9*, 543–552.
(7) Abraham, N. G.; Kappas, A. Pharmacological and clinical aspects of heme oxygenase. *Pharmacol. Rev.* **2008**, *60*, 79–127.
(8) Fang, J.; Akaike, T.; Maeda, H. Antiapoptotic role of heme oxygenase (HO) and the potential of HO as a target in anticancer treatment. *Apoptosis* **2004**, *9*, 27–35.
(9) Fang, J.; Sawa, T.; Akaike, T.; Greish, K.; Maeda, H. Enhancement of chemotherapeutic response of tumor cells by a heme oxygenase inhibitor, pegylated zinc protoporphyrin. *Int. J. Cancer* **2004**, *109*, 1–8.
(10) Fang, J.; Sawa, T.; Akaike, T.; Akuta, T.; Sahoo, S. K.; Khaled, G.; Hamada, A.; Maeda, H. In vivo antitumor activity of pegylated zinc protoporphyrin: targeted inhibition of heme oxygenase in solid tumor. *Cancer Res.* **2003**, *63*, 3567–3574.
(11) Vlahakis, J. Z.; Kinobe, R. T.; Bowers, R. J.; Brien, J. F.; Nakatsu, K.; Szarek, W. A. Synthesis and evaluation of azalanstat analogues as heme oxygenase inhibitors. *Bioorg. Med. Chem. Lett.* **2005**, *15*, 1457–1461.
(12) Vlahakis, J. Z.; Kinobe, R. T.; Bowers, R. J.; Brien, J. F.; Nakatsu, K.; Szarek, W. A. Imidazole−dioxolane compounds as isozyme-selective heme oxygenase inhibitors. *J. Med. Chem.* **2006**, *49*, 4437–4441.
(13) Roman, G.; Riley, J. G.; Vlahakis, J. Z.; Kinobe, R. T.; Brien, J. F.; Nakatsu, K.; Szarek, W. A. Heme oxygenase inhibition by 2-oxy-substituted 1-(1*H*-imidazol-1-yl)-4-phenylbutanes: effect of halogen substitution in the phenyl ring. *Bioorg. Med. Chem.* **2007**, *15*, 3225–3234.
(14) Kinobe, R. T.; Vlahakis, J. Z.; Vreman, H. J.; Stevenson, D. K.; Brien, J. F.; Szarek, W. A.; Nakatsu, K. Selectivity of imidazole−dioxolane compounds for in vitro inhibition of microsomal haem oxygenase isoforms. *Br. J. Pharmacol.* **2006**, *147*, 307–315.
(15) Vlahakis, J. Z.; Hum, M.; Rahman, M. N.; Jia, Z.; Nakatsu, K.; Szarek, W. A. Synthesis and evaluation of imidazole−dioxolane compounds as selective heme oxygenase inhibitors: effect of substituents at the 4-position of the dioxolane ring. *Bioorg. Med. Chem.* **2009**, *17*, 2461–2475.
(16) Rahman, M. N.; Vlahakis, J. Z.; Szarek, W. A.; Nakatsu, K.; Jia, Z. X-ray crystal structure of human heme oxygenase-1 in complex with 1-(adamantan-1-yl)-2-(1*H*-imidazol-1-yl)ethanone: a common binding mode for imidazole-based heme oxygenase-1 inhibitors. *J. Med. Chem.* **2008**, *51*, 5943–5952.
(17) Sugishima, M.; Higashimoto, Y.; Oishi, T.; Takahashi, H.; Sakamoto, H.; Noguchi, M.; Fukuyama, K. X-ray crystallographic and biochemical characterization of the inhibitory action of an imidazole−dioxolane compound on heme oxygenase. *Biochemistry* **2007**, *46*, 1860–1867.
(18) Schuller, D. J.; Wilks, A.; Ortiz de Montellano, P. R.; Poulos, T. L. Crystal structure of human heme oxygenase-1. *Nat. Struct. Biol.* **1999**, *6*, 860–867.
(19) Lad, L.; Schuller, D. J.; Shimizu, H.; Friedman, J.; Li, H.; Ortiz de Montellano, P. R.; Poulos, T. L. Comparison of the heme-free and -bound crystal structures of human heme oxygenase-1. *J. Biol. Chem.* **2003**, *278*, 7834–7843.
(20) Schuller, D. J.; Wilks, A.; Ortiz de Montellano, P. R.; Poulos, T. L. Crystallization of recombinant human heme oxygenase-1. *Protein Sci.* **1998**, *7*, 1836–1838.
(21) Wilks, A.; Ortiz de Montellano, P. R. Rat liver heme oxygenase. High level expression of a truncated soluble form and nature of the meso-hydroxylating species. *J. Biol. Chem.* **1993**, *268*, 22357–22362.
(22) Wilks, A.; Black, S. M.; Miller, W. L.; Ortiz de Montellano, P. R. Expression and characterization of truncated human heme oxygenase (hHO-1) and a fusion protein of hHO-1 with human cytochrome P450 reductase. *Biochemistry* **1995**, *34*, 4421–4427.
(23) Wang, J.; Niemevz, F.; Lad, L.; Huang, L.; Alvarez, D. E.; Buldain, G.; Poulos, T. L.; de Montellano, P. R. Human heme oxygenase oxidation of 5- and 15-phenylhemes. *J. Biol. Chem.* **2004**, *279*, 42593–42604.
(24) Otwinowski, Z.; Minor, W. Processing of X-ray diffraction data collected in oscillation mode. *Macromol. Crystallogr., Part A* **1997**, *276*, 307–326.
(25) Collaborative Computational Project, N. 4. The CCP4 suite: programs for protein crystallography. *Acta Crystallogr., Sect. D.: Biol. Crystallogr.* **1994**, *50*, 760−763.
(26) Schuttelkopf, A. W.; van Aalten, D. M. PRODRG: a tool for high-throughput crystallography of protein−ligand complexes. *Acta Crystallogr., Sect. D: Biol. Crystallogr.* **2004**, *60*, 1355–1363.
(27) Adams, P. D.; Grosse-Kunstleve, R. W.; Hung, L. W.; Ioerger, T. R.; McCoy, A. J.; Moriarty, N. W.; Read, R. J.; Sacchettini, J. C.; Sauter, N. K.; Terwilliger, T. C. PHENIX: building new software for automated crystallographic structure determination. *Acta Crystallogr., Sect. D: Biol. Crystallogr.* **2002**, *58*, 1948–1954.
(28) Emsley, P.; Cowtan, K. Coot: model-building tools for molecular graphics. *Acta Crystallogr., Sect. D: Biol. Crystallogr.* **2004**, *60*, 2126–2132.
(29) DeLano, W. L. The PyMOL Molecular Graphics System; DeLano Scientific: Palo Alto, CA, 2002.
(30) Carugo, O.; Argos, P. Accessibility to internal cavities and ligand binding sites monitored by protein crystallographic thermal factors. *Proteins* **1998**, *31*, 201–213.
(31) Yuan, Z.; Zhao, J.; Wang, Z. X. Flexibility analysis of enzyme active sites by crystallographic temperature factors. *Protein Eng.* **2003**, *16*, 109–114.